

Mechanical damage detection using magnetic flux leakage tools: modeling the effect of dent geometry and stresses

Vijay Babbar*, James Bryne, Lynann Clapham

Physics Department, Queen's University, Stirling Hall, Kingston, Ont., Canada K7L 3N6

Received 1 October 2004; accepted 15 December 2004

Available online 3 February 2005

Abstract

We have used three-dimensional (3D) magnetic finite element analysis (FEA) to simulate the MFL signal from a circular dent geometry with associated residual stresses. Strain distribution information around the dent was obtained from an earlier work using finite element structural modeling. In the magnetic FEA dent model, the localized residual stresses were simulated by assigning appropriate values of magnetic anisotropy to the relevant magnetic regions. The simulated flux leakage patterns were found to be in good agreement with the experimentally observed MFL patterns associated with dent shape as well as with the stress effects from the dent.

© 2005 Elsevier Ltd. All rights reserved.

Keywords: Finite element analysis; Magnetic flux leakage; Nondestructive evaluation; Stress

1. Introduction

The Magnetic Flux Leakage (MFL) inspection method is the most cost effective technique for detecting corrosion and metal loss in in-service pipelines. The principle of the technique is relatively straightforward—a magnetic field is induced in the pipe wall using permanent magnets, with flux forced out to ‘leak’ out of the wall in the presence of a metal loss defect. This ‘leakage flux’ is then detected by a Hall probe or coil at the pipe wall surface. MFL is stress-sensitive, therefore recent attention has focused on using these tools to detect mechanical damage—dents or gouges in the pipe caused by rocks, terrain slippage or a third party interference. MFL signals from dents are very difficult to interpret, however, since the signal arises from both geometry and stress effects.

Magnetic finite element analysis (FEA) has become a powerful modeling tool for studying MFL signals from corrosion defects [1–4]. In this paper, we apply magnetic FEA to the case of circular dents in a plate sample. The FEA method is particularly useful because it can be used to study

separately, and combined, MFL signals from the defect geometry as well as the associated stresses.

In a previous paper [5], we reported the effect of local dent-induced stresses on MFL signals studied by using both FEA modeling and experimental methods. The present paper continues this analysis, examining the effects of both dent geometry and localized residual stresses on MFL.

2. The models

2.1. Structural FEA model

Since the MFL signals are affected not only by the geometry of dents, but also by the presence of stresses in the dented region, it is necessary to obtain information about these stress patterns. Earlier studies [6] showed that the MFL signals around dents are sensitive to the elastic residual strain, but not plastic deformation. This is true up to about 30% strain, consistent with strain levels around typical dents. The first stage of our work, therefore, involved studying the elastic residual strain patterns around a dent using finite element structural modeling. A nonlinear structural FEA model using ANSYS software was used for simulating three-dimensional (3D) residual stress

* Corresponding author. Tel.: +1 613 533 6000x74782; fax: +1 613 533 6463.

E-mail address: babbar@physics.queensu.ca (V. Babbar).

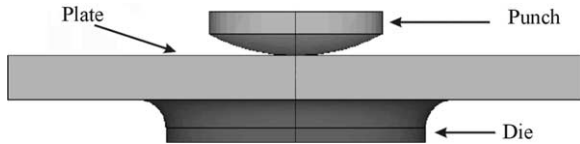


Fig. 1. Geometry of the FEA structural model.

profiles in a dented plate. The model geometry used and the results obtained from FEA stress analysis were reported in an earlier paper [5] and are reproduced in Figs. 1 and 2, respectively. A brief description of the model is given below.

The model consists of a dent of diameter 12 mm and depth 3 mm produced by a round-bottomed punch on a mild steel plate of dimensions $40\text{ mm} \times 40\text{ mm} \times 3\text{ mm}$ supported on a die of hole diameter 18 mm. Only one-quarter of the model is necessary due to symmetry considerations. The interfaces between the die and the plate, and between the plate and the punch are modeled using an automatic surface-to-surface contact algorithm, which uses the material properties of both contacting surfaces to calculate the stiffness of the contact elements. An elastic Coulomb friction law is assumed and a friction coefficient of 0.15 is assigned to the contacting surfaces. The stress–strain behavior of the material is described by a bilinear total stress–total strain curve starting at the origin and with positive stress and strain values. A piecewise linear elastic-perfect plastic material model is assumed for the plate with following parameters: Young's modulus 207 GPa, yield strength 160 MPa, tangent modulus 0.112 GPa, Poisson's ratio 0.290 and density 7900 kg m^{-3} .

Fig. 2(a)–(c) show the normal residual stresses in the x and y directions and the shear stresses, respectively. The normal z -directional stresses are not considered here since they are an order of magnitude less. In the dent rim region the x and y stresses are more concentrated near the sidewalls of the dent, however, they are present everywhere in the dent base. The shear stresses are mainly present near the middle part of the dent rim region. Also, through the thickness, the upper half of the sloping dent wall in the dent rim region exhibits tensile stresses, and the lower half compressive stresses. In the dent base region, the through-thickness pattern is opposite; i.e. the upper half is compressive and the lower half tensile.

2.2. Magnetic FEA model

Infolytica's MagNet6 software is used for magnetic finite element modeling. A quarter model of a dent was drawn by making use of the four-fold symmetry of the problem and is shown schematically in Fig. 3. It consists of a steel plate of dimensions $54\text{ mm} \times 108\text{ mm} \times 4\text{ mm}$, which has a quarter dent of depth 4 mm at one of the corners as shown. The sloping wall of the dent lies within a quarter ring of inner radius 12 mm and outer radius 28 mm. Two vertical planes

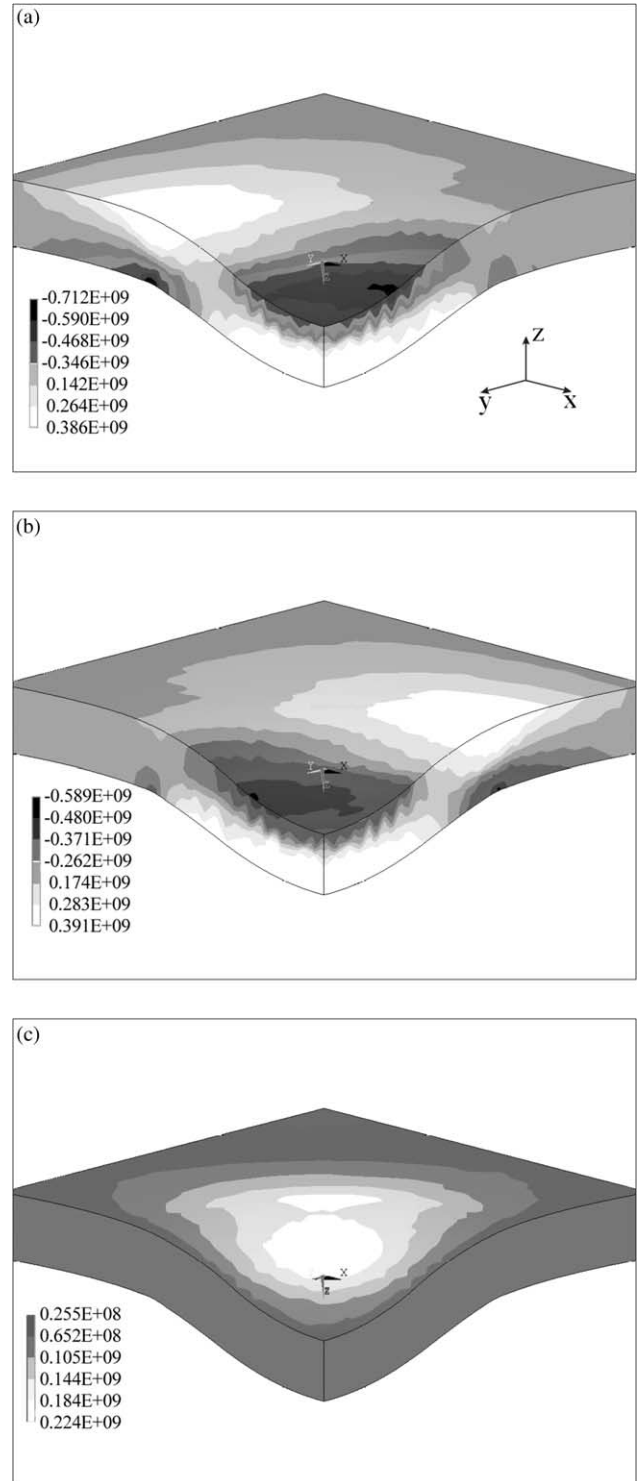


Fig. 2. Residual stresses in a $20\text{ mm} \times 20\text{ mm} \times 3\text{ mm}$ quarter section of the structural model. (a) Normal stresses in the x -direction, (b) normal stresses in the y -direction, and (c) shear stresses.

divide the dent wall into three vertical blocks which are further sub-divided into four parallel sections of width 1 mm each all along the shape of the wall, thus making a total of 12 dent rim segments. The base region of uniform thickness 4 mm is divided into four horizontal sections.

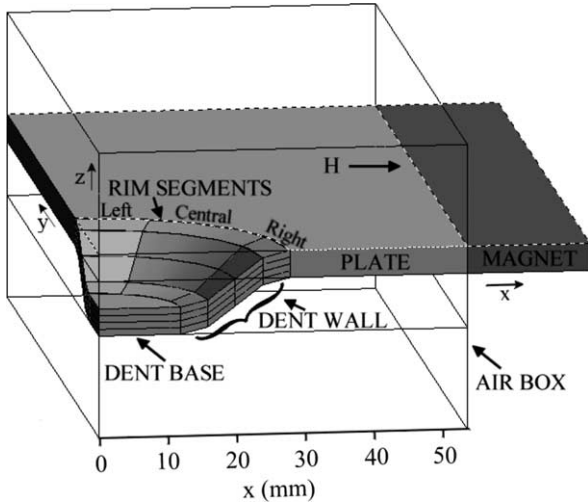


Fig. 3. Schematic 3D view of the quarter magnetic FEA model showing the dent wall, dent base and dent rim segments.

Different magnetic properties along the orthogonal x , y and z directions can be assigned to these segments to account for the local residual strains. An NdFeB magnet of dimensions $18\text{ mm} \times 108\text{ mm} \times 4\text{ mm}$ and coercivity $1.6 \times 10^6\text{ A m}^{-1}$ is used to magnetize the steel plate in the x -direction. This particular combination of the plate dimensions, magnet dimensions and coercivity has been used to produce a flux density of about 1.8 T in the plate, which corresponds to a high magnetization level during an actual MFL inspection.

The radial MFL signal is estimated by examining the radial component of the magnetic field in the air above (topside) or below (bottomside) the plate. The topside data is taken over a single horizontal plane at a distance of 0.5 mm above the plate. The bottomside data is taken along the sloping convex surface of the dent profile at a distance of 0.5 mm away from the plate. The data from the convex surface is obtained by considering data from the set of parallel planes underneath the plate and then selecting the points adjacent to the surface. Finally, it should be noted that the topside results correspond to the MFL results that would be obtained from the outside wall of a pipe, and the bottomside results would correspond to the inside wall. The bottom side results have greater significance for industry since MFL inspection is internal to the pipe and samples the signal at the inside pipe wall surface.

The way in which stress effects are accounted for in the magnetic FEA model is explained below.

2.2.1. Accounting for stress using magnetic anisotropy variations

Since steel, in general, has a positive magnetostriction coefficient, 180° domains will tend to align their magnetic easy axis closest to, and ultimately rotate it towards, the direction of the applied tensile stress. This increases the magnetic permeability in the tensile stress direction. Conversely, an applied compression will increase

the magnetic permeability in a direction transverse to the stress axis.

The Infolytica MagNet6 software allows for 3D nonlinear anisotropic FEA calculations with customer-supplied magnetization functions. Since high axial fields are used, it is assumed that magnetization must always be in the field direction, and that it can be described as an arc tangent of the field, with the B – H curve approximated as

$$B = \mu_0 \left[\frac{2M_s}{\pi} \tan^{-1}(H/H_k) + H \right] \quad (1)$$

where μ_0 is the permeability of free space, H_k is a directionally dependent anisotropy parameter, M_s is the saturation magnetization equal to 1700 kA m^{-1} (for this steel), and H is assigned to be $27,500\text{ A m}^{-1}$. This equation is used to calculate the components of B by using the values of H_k in different directions.

According to (1), the maximum permeability μ_m can be shown to be

$$\mu_m = \mu_0 \left(\frac{2M_s}{\pi H_k} + 1 \right) \quad (2)$$

Thus, smaller values of H_k imply higher permeability.

Since tensile stress increases and compressive stress decreases the permeability in the stress direction, we vary H_k in a specific (x , y , or z) direction to simulate applied stress. For example, one can simulate a tensile stress in the y -direction by decreasing H_k in that direction and/or by increasing H_k along the other two orthogonal directions. In general, the anisotropy parameter in any given direction is expressed as

$$H_k = H_{kx}\alpha_x^2 + H_{ky}\alpha_y^2 + H_{kz}\alpha_z^2 \quad (3)$$

where H_{kx} , H_{ky} and H_{kz} are the three orthogonal anisotropy parameters, and α_x , α_y , and α_z are the cosines of the field vector in that direction.

In the present study, we have used $H_{kx} = H_{ky} = H_{kz} = 9000\text{ A m}^{-1}$ for simulating an isotropic (no stress) steel section of the model. Solution of the model indicates that this H_k value corresponds to a relative permeability of 50.4 and a flux density of 1.74 T inside the steel plate for an applied axial field of about $27,500\text{ A m}^{-1}$. Outside the plate, the radial flux density in this case is calculated to be $\mu_0 H = 0.038\text{ T}$.

As mentioned before, tensile or compressive stresses are incorporated by assigning $H_{k(x,y,z)}$ values less than or greater than 9000 A m^{-1} , respectively. We simulate tensile stresses by reducing H_k by a factor of 4.5. For simulating compressive stresses, we increase H_k by a factor of 6.5 ($\cong 4.5 \times 1.5$). This is done because, as revealed by the structural FEA model, the maximum compressive stress is about 1.5 times higher than the maximum tensile stress.

The MFL results for various geometry and stress combinations are considered below. Both topside and

bottomside results are included in the present study; however, because of their widespread use by the industry, the bottomside results are described in greater detail.

2.3. Bottomside results

2.3.1. Effect of dent geometry only (no stress contribution)

The effect of dent geometry alone was simulated by making the magnetic behavior isotropic and H_k equal to 9000 A/m for all regions of the model shown in Fig. 3. The contour map of the radial bottomside MFL signal, obtained after background subtraction of the corresponding data for the ‘no dent’ case (basically a flat plate), is shown in Fig. 4. The broken lines on the map show all the 12 segments of the dent (shown in Fig. 3) as viewed from the top. The region inside the innermost quarter circle represents the dent base. The results seen in Fig. 4 indicate that the flux is initially forced out at the axial edge of the dent, then re-enters again just before the dent base.

2.3.2. Effect of stresses only (no geometry contribution)

The stress modeling results shown in Fig. 2 indicates a continuous stress distribution, as expected. This implies a continuous spatial change in magnetic anisotropy, however, this could not be practically implemented in the model. As an alternative, the model was assigned constant H_k parameters (in directions x , y , and z) in each of the 13 discrete regions—12 dent rim regions and the dent base, as mentioned earlier. Results associated with assigning ‘stresses’ to specific regions are discussed below.

2.3.2.1. Rim stresses in left and right blocks. Fig. 2(a) and (b) indicate that most of the normal ‘dent rim’ stresses are located at the outside of the rim—corresponding the outer two rings of the model in Fig. 3. The stresses in the two inner rim segments are very small in comparison and are, therefore, ignored in the model.

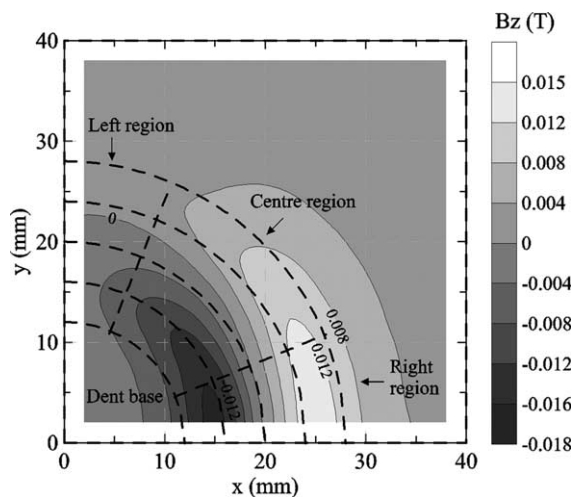


Fig. 4. Bottomside contour map obtained at 0.5 mm underneath the dented steel plate sample showing the effect of dent geometry alone.

Consistent with the results of Fig. 2(a) and (b), the Right segments were assigned x -directional stresses, while the Left segments were assigned y -directional stresses. Segments in the upper two sections of the plate were assigned tensile stresses and those in the lower two sections compressive stresses.

Radial MFL patterns resulting from a stress-only distribution were obtained by assigning stresses to the model of Fig. 3, obtaining the results, and then subtracting off the ‘geometry MFL signal’ (i.e. the signal shown in Fig. 4). Fig. 5(a) shows the final ‘stress-only’ result for this case, indicating a positive peak located near the Left/Centre block boundary. Further studies indicate that this peak was primarily associated with the compressive stress in the bottom sections. Furthermore, the anisotropy of the Right segments, being tensile and in the direction of the applied field, was found to make no contribution to the MFL signal. This is consistent with our earlier reports of the stress-only results [5].

2.3.2.2. Rim stresses in the center block. The stress pattern of Fig. 2(c) reveals shear stresses in the Center block, again mainly in the outer part of the rim, and primarily tensile at the top and compressive at the bottom. Although the present version of the Magnet software does not support the assignment of shear stresses, an approximation was made by simulating stresses along the [110] direction of the Central outer rim segments. The MFL patterns generated by the Central outer rim stresses alone are shown in Fig. 5(b). The pattern consists of a negative peak region centered on the Left/Central block boundary and a positive one on the Central/Right boundary. The reason for obtaining this type of pattern will be considered in a subsequent section.

2.3.2.3. Dent base stresses. The structural modeling results of Fig. 2(a) and (b) indicate that at the dent base, normal stresses are present in both x and y directions, compressive at the top and tensile at the bottom. In the magnetic FEA model, these stresses were simulated by assigning x and y anisotropies to the four layers of the dent base such that the top two sections behave as xy -compressive and the bottom two as xy -tensile. The resulting leakage field pattern is shown in Fig. 5(c), and consists of a single positive peak. This is similar to the pattern of Fig. 5(a), and additional studies indicated that it was dominated by the compressive, rather than the tensile, stress influence.

2.3.2.4. Effect of combined stress. Fig. 5(d) shows the combined effect of all dent rim and base stresses. It is effectively the algebraic sum of all the stress effects shown in Figs. 5(a)–(c). As mentioned above, our results indicate that the radial MFL signal is most highly sensitive to any compressive stresses lying perpendicular to the flux path. These compressive stresses effectively lower the steel permeability, thus forcing flux out of the pipe. Stress peaks,

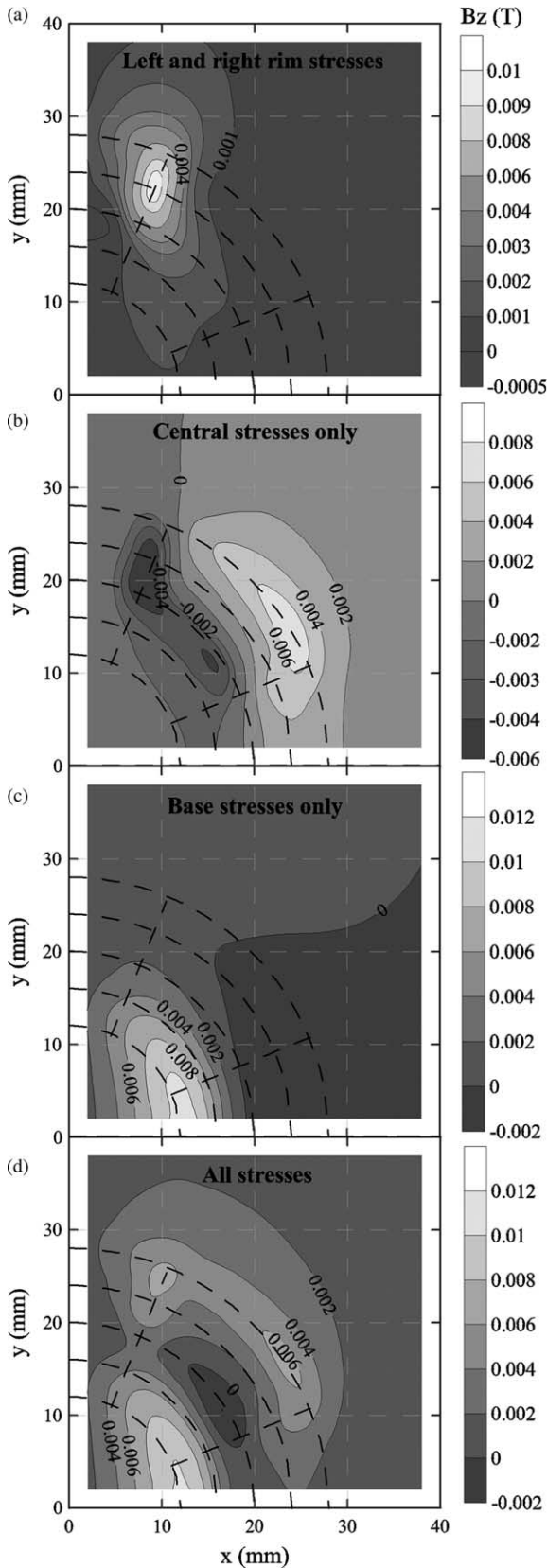


Fig. 5. Bottomside contour maps at 0.5 mm underneath the dented steel plate sample showing the effect of tensile as well as compressive stresses in (a) side blocks, (b) central block, (c) base region, and (d) all the above three cases.

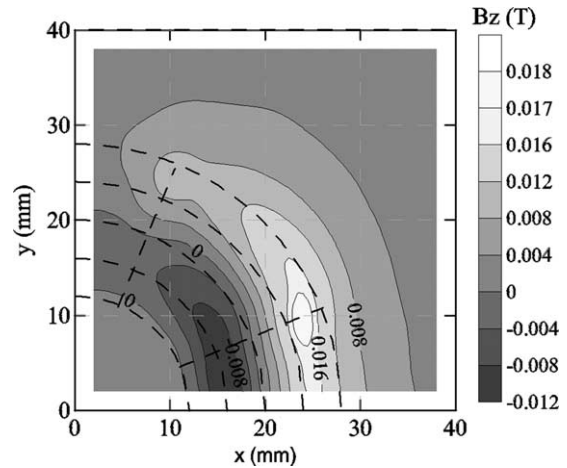


Fig. 6. Bottomside contour maps at 0.5 mm underneath the dented steel plate sample showing the combined effect of dent geometry and stresses.

therefore, tend to be associated primarily with compressive stress regions.

2.3.3. Effect of dent geometry and stresses

Fig. 6 shows the combined effect of dent shape and all the stresses, which can be seen as an algebraic combination of the shape effect pattern of Fig. 4 and stress pattern of Fig. 5(d). Since the geometry effect dominates that of the stresses, the combined pattern retains most of the features of the shape effect pattern except for a distinct positive peak appearing near the boundary of the Central/Right region. This region is very important, as it is one of the characteristic features of the experimental pattern to be discussed below.

2.4. Topside results

The topside results are obtained along the horizontal plane 0.5 mm above the top of the plate. The topside combined stress-only pattern is shown in Fig. 7(a). This is very similar to the corresponding bottomside pattern (Fig. 5(d)) except that the signal from the base region is very weak due to large distance of the topside surface from the dent base. Fig. 7(b) shows the combined stress and geometry MFL pattern; again this is similar to combined bottomside result (Fig. 6) except for the polarity and the smaller influence of the base region. The combined geometry and stress effect pattern (Fig. 7(b)) is also similar to the bottomside pattern except for the base region.

3. Experimental details and results

Experimental MFL testing was carried out for comparison with the FEA modeling results. Samples of mild steel of approximate dimensions 200 mm × 150 mm × 3 mm were first sanded and then heat-treated at 500 °C for 1 h to remove any residual stresses that might be present before denting. An experimental tool and die of dimensions similar to that

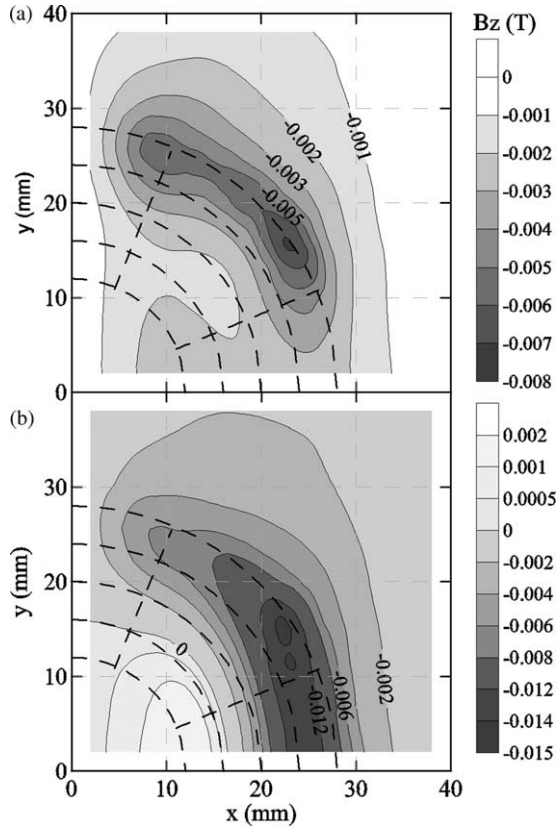


Fig. 7. Topside contour maps in a plane at 0.5 mm above the upper surface of the dented steel plate sample showing (a) effect of stresses only, and (b) combined effect of dent geometry and stresses.

used in the FEA stress model (Fig. 1) was used to produce dents. These dents were made by using a hydraulic press at a ram speed of 6 mm/s in constant displacement mode with an applied force of about 16–17 kN. A number of dents with dent depths of 0.5–8 mm and diameters 12–25 mm were produced.

MFL measurements were made after denting the top surface of the plate. The MFL experimental arrangement was similar to that described in a previous work [7] except that the sample in the present work was a flat plate instead of a pipe. Magnetic flux was introduced into the plate by an NdFeB permanent magnet circuit. The MFL signal (radial component) was detected by using a Hall probe, which was scanned over a 40 mm × 40 mm area around the dent on the topside and the bottom side of the dent. Finally, a 3D plotting package (Surfer 7.0) from Golden Software was used for obtaining surface and contour maps.

The experimental results for the combined geometry and stress effects are shown in Fig. 8; bottomsides results are shown in Fig. 8(a) and topside results in Fig. 8(b). The corresponding FEA results have been shown in Figs. 6 and 7(b), respectively. Please note that the flux density in Fig. 8 is given in Gauss instead of Tesla as in FEA plots. Furthermore, the experimental bottomsides results (Fig. 8(a)) have opposite polarity compared to FEA results, due to the Hall probe

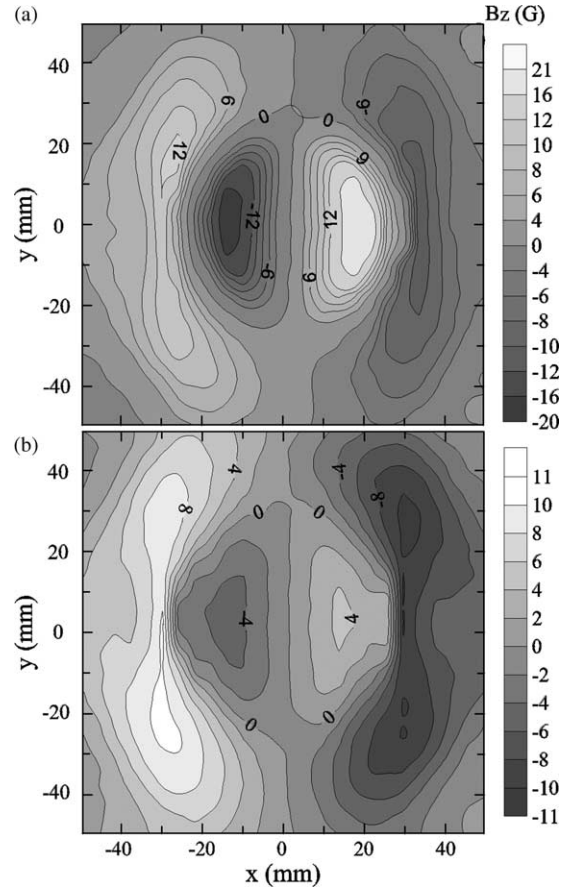


Fig. 8. Experimental contour maps of the dented steel plate sample showing the effect of geometry as well as stresses: (a) bottomsides results, and (b) topside results.

orientation with respect to the sample. In general, there is an excellent matching between the experimental and modeled results. Like the modeled results, the topside experimental results also show a weaker MFL signal from the base region than the corresponding bottomsides results. It is also apparent that the shoulder peaks in the experimental results appear mainly due to the stress effect, while the rest of the pattern corresponds to the geometry of the dent.

4. Summary and conclusions

We have examined dent-induced radial MFL signals by modeling the effects of dent geometry and residual stresses in the dent wall and dent base regions. The information about the nature and magnitude of stresses was obtained by modeling the elastic residual stress patterns around a dent using finite element structural analysis. This stress information is incorporated into the magnetic FEA model by adjusting the H_k permeability variable according to the modeled stress results. The MFL signal resulting from different stressed regions have been studied separately and in combination with the shape effect. The shape effect signal is larger than the stress effect signal, although the stress

effect produces a distinctive ‘stress peak’ in the dent rim region. Furthermore, the MFL signal has greater sensitivity for compressive stresses than for tensile stresses. The bottomside patterns exhibit a close resemblance to the corresponding topside patterns (although opposite in polarity). Overall, the combined shape and stress effect FEA pattern shows an excellent matching with the corresponding experimental pattern, particularly considering the simplifications in the modeling approach.

References

- [1] Ida N, Lord W. 3-D finite element predictions of magnetostatic leakage fields. *IEEE Trans Magn* 1983;MAG-19(5):2260–5.
- [2] Atherton DL. Finite element calculations and computer measurements of magnetic flux leakage patterns from pits. *Br J NDT* 1988;30(3): 159–62.
- [3] Ivanov PA, Zhang Z, Yeoh CH, Udpa L, Sun Y, Udpa SS, et al. Magnetic flux leakage modeling for mechanical damage in transmission pipelines. *IEEE Trans Magn* 1998;MAG-34(5):3020–3.
- [4] Mao W, Mandache C, Clapham L, Atherton DL. The effect of bulk stresses on magnetic flux leakage signals. *Insight* 2001;43(10): 688–91.
- [5] Babbar V, Shiari B, Clapham L. Mechanical damage detection with magnetic flux leakage tools: modeling the effect of localized residual stresses. *IEEE Trans Magn* 2004;MAG-40(1):43–9.
- [6] Stefanita C-G, Atherton DL, Clapham L. Plastic versus elastic deformation effects on magnetic Barkhausen noise in steel. *Acta Mater* 2000;48:3545–51.
- [7] Babbar V, Clapham L. Residual MFL—a possible tool for studying pipeline defects. *J Nondestr Eval* 2003;22(4):117–25.